

Article

Construction and Investigation of a Filtration Efficiency Test System for High-Efficiency Filter Materials Based on Mass Concentration

Fang Wei ^{1,2}, Yun Liang ¹, Hao Wang ², Mengxiang Hu ^{1,2}, Lingyun Wang ^{2,*}, Desheng Wang ² and Min Tang ^{1,*} 

¹ School of Light Industry and Engineering, South China University of Technology, Guangzhou 510640, China; 202120129085@mail.scut.edu.cn (F.W.); liangyun@scut.edu.cn (Y.L.); 201920126892@mail.scut.edu.cn (M.H.)

² State Key Laboratory of NBC Protection for Civilian, Beijing 100191, China; wanghao_scut@126.com (H.W.); deshen1982@163.com (D.W.)

* Correspondence: wangly817@163.com (L.W.); tangmin88@scut.edu.cn (M.T.)

Abstract: Protection from nuclear biochemical aerosol and air pollution pays attention to aerosol mass concentration. The concentration of upstream aerosol of the commonly used filtration efficiency detection device for high-efficiency filter materials is low, making it insufficient for detecting the filtration efficiency of high-efficiency filter materials. This study designed and built a set of filtration efficiency detection devices for high-efficiency filter materials based on mass concentration. By adjusting the oil bath temperature, injection pressure, the degree of spiral-separator separation, as well as the number and size of nozzles, we investigated the effects of each condition on the concentration and particle size distribution of aerosol generation. As a result, the oil mist generator of the device can stably generate high-concentration aerosol with a mass concentration of up to 1587.9 mg/m³ and a number concentration of up to 10⁷–10⁸ P/cm³. The high-concentration aerosol generated can meet the E11–U15 filter material performance requirements.

Keywords: mass concentration; high-concentration aerosol; high efficiency; filtration efficiency; test system



Citation: Wei, F.; Liang, Y.; Wang, H.; Hu, M.; Wang, L.; Wang, D.; Tang, M. Construction and Investigation of a Filtration Efficiency Test System for High-Efficiency Filter Materials Based on Mass Concentration. *Processes* **2024**, *12*, 981. <https://doi.org/10.3390/pr12050981>

Academic Editor: Ireneusz Zbicinski

Received: 3 April 2024

Revised: 8 May 2024

Accepted: 9 May 2024

Published: 12 May 2024



Copyright: © 2024 by the authors. Licensee MDPI, Basel, Switzerland. This article is an open access article distributed under the terms and conditions of the Creative Commons Attribution (CC BY) license (<https://creativecommons.org/licenses/by/4.0/>).

1. Introduction

With the rapid development of social industrialization, many fine particulate matter emissions are generated, leading to a series of air pollution problems and a significant burden on environmental safety and public health [1–3]. High air mobility leads to the long duration and comprehensive coverage of pollution in the atmospheric environment [4]. Fine particulate matter suspended in the air can easily be deposited in the human body through respiration and other effects. It can lead to respiratory diseases, and nervous system disorders, among other problems, posing a serious hazard to human health [5,6]. In the military field, nuclear, biological, and chemical aerosols pose a deadly threat to people's health and safety.

High-efficiency particulate air (HEPA) filters can effectively intercept fine particle pollutants in air. Filter efficiency is the most important index for evaluating air filters, and the efficiency of an air filter is determined by filter materials [7–9]. Because of the different properties of aerosols that need to be considered in various settings, the test methods of filter materials used in other industries are also different. In the fields of nuclear biochemical aerosol protection and air pollution, more attention has been paid to the mass concentration of aerosols. Air pollution is strongly associated with human health and particulate matter (PM) in the air entering the human body mainly through breathing. Toxicological studies have shown that not only is there an association between environments with high concentrations of particulate matter and cardiopulmonary diseases in humans, but also environments with low concentrations of air pollution can significantly

affect human health. In personal protection against respiratory occupational hazards, there is a need to focus on the mass concentration limit thresholds/permissible exposure limits (TLV/PEL) of the environment, and the transmittance measurements specified in the current NIOSH standard are based on mass concentration detection methods. In the field of NBC protection, the agent exists in three main types: liquid droplets, microdroplets, and aerosols and vapors when a toxic agent is administered. The toxic dose of a chemical agent is expressed as the product of the mass concentration of the agent and the exposure time. The half incapacitating dose (ICt50) and the half-lethal dose (LCt50) are expressed through mass concentration [10]. Due to the fact that NBC aerosols may contain radioactive and toxic chemicals, highly toxic or radioactive substances may cause serious health problems even if the number of particles is small, so more attention is paid to the mass concentration of the aerosol rather than the number concentration. Therefore, building a filtration efficiency testing system for high-efficiency filter materials based on mass concentration is a great significance.

Test methods based on mass concentration mainly include the sodium-flame, DOP (Diocetyl Phthalate), and oil-mist methods. Walton proposed the sodium-flame method in 1941. However, NaCl becomes cubic after crystallization, which is inconsistent with the state of the agent used in military applications. This method is generally not used for detecting poison aerosols in protective filter materials [11]. The DOP method originated in the United States, and the TSI 8130 (automatic filter material tester which is manufactured by TSI, Inc.) using the cold DOP method is the most commonly used filter material test stand. The operation is fast and straightforward. However, the aerosol concentration is low, and the number concentration of upstream aerosol is 5×10^6 P/cm³. Moreover, the highest mass concentration of oily aerosol is 200 mg/m³. Due to the low aerosol concentration, fewer aerosol particles will be available to pass through the high-efficiency filter material when tested, affecting the test results. The oil-mist method was proposed by the Soviet Union and gradually developed into a standard test method for efficient filter materials in China. The oil-mist method can produce high concentrations of aerosol, which can meet the performance requirements of high-efficiency and ultra-efficient filter materials.

Different test methods have their advantages and scope of application, so many researchers have conducted work that make comparisons between them. Eninger et al. investigated the validity of photometric measurements of nanoparticulate matter. The results showed that the current National Institute for Occupational Safety and Health (NIOSH) method of filter media detection based on mass concentration cannot sensitively measure nanoparticles in the environment, because nanoparticulate matter light scattering intensity is weak and the instrument is not sensitive enough. Its accuracy and sensitivity for nanoparticle concentration measurement may not be high enough [12]. Gregory et al. explored the effect of the NaCl and DOP aerosol particle size and flow rate on the efficiency of different types of filter materials. The study showed that the most penetrating particle size of the filter material was correlated with the flow rate and the type of filter material [13]. Li et al. compared the penetration rates of different filter media in different laboratories based on the number concentration of the particles, surface area concentration, and mass concentration of particulate matter using different test methods. The results showed that the data obtained in different laboratories were reproducible and comparable, and the filtration efficiencies of polydispersed aerosols and monodispersed aerosols measured by scanning the mobility particle sizer (SMPS) were similar to those of monodispersed aerosols. The results of the monodisperse aerosol test are in good agreement [14].

The TSI 8130 and the most easily penetrating particle-size test stand were commonly used. However, due to a low upstream aerosol concentration, they can influence the detection of high-efficiency filter material above grade E11 (filtration efficiencies of 95% or more) [15]. In this study, we designed a filtration efficiency test system for high-efficiency filter materials based on a high-concentration aerosol. We determined the aerosol generation conditions by exploring the effects of the oil bath temperature, injection pressure, spiral-separator separation degree, and nozzle number and size on aerosol concentration and size

distribution. The oil mist generator of the device can stably generate high-concentration aerosol with a mass concentration of up to 1587.9 mg/m^3 and a number concentration of up to $10^7\text{--}10^8 \text{ P/cm}^3$. The high-concentration aerosol generated can allow the test system to meet high-efficiency and ultra-efficient filter material performance requirements. Therefore, the test system will be more suitable for the characterization of filter media for nuclear biochemical aerosol protection, air pollution, and other fields.

2. System Composition

2.1. Composition of the Filter Efficiency Test Stand Based on Mass Concentration

By analyzing the current commercial filter material test stand and based on the relevant research [16–20], the filtration efficiency test stand was found to mainly comprise a clean gas source supply system, an oil-mist aerosol generation system, a filter clamp system, and an aerosol test system. Combined with the GB 6165-2021 test standard [21], we designed and built a filtration efficiency test stand based on mass concentration, as shown in Figure 1.

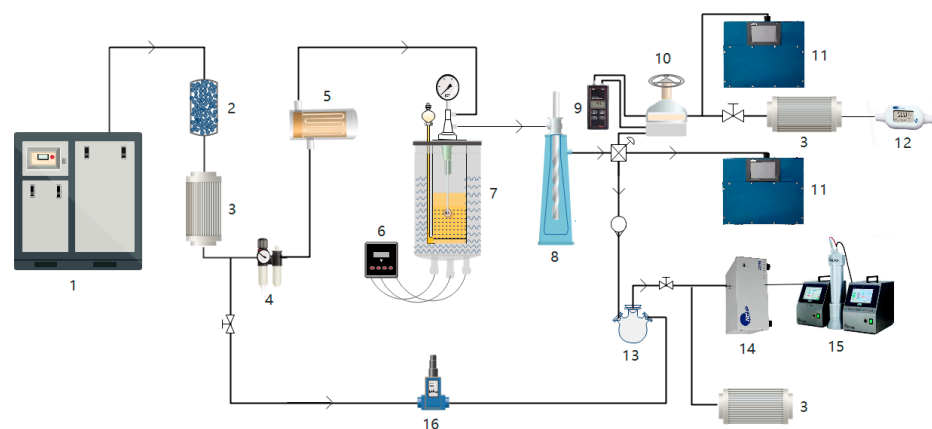


Figure 1. Schematic diagram of the filtration efficiency test stand based on mass concentration. 1—Air compressor; 2—Dryer; 3—HEPA filter; 4—Pneumatic single connector; 5—Air heater; 6—Temperature-sensing controller; 7—Oil mist generator; 8—Spiral separator; 9—Differential pressure meter; 10—Filter fixture; 11—Light meter; 12—Flow meter; 13—Mixer; 14—Electrostatic neutralizing; 15—Scanning electric mobility particle size spectrometer; 16—Flow controller.

2.1.1. Clean Air Supply System

The clean air supply system comprises three HEPA filters. The first HEPA filter is installed in the outlet of the air compressor to ensure that the gas is dry and clean. The second HEPA filter is installed before the filtered gas discharge to ensure that part of the particulate matter passes through the efficient filter material and does not enter the loss equipment in the flowmeter. The third HEPA filter is installed in the bypass to ensure that exhaust gas does not pollute air and protect the operator.

2.1.2. Oil-Mist Aerosol Generation System

The aerosol generator is an oil-bath spray generator. As shown in Figure 2, the main components of the occurrence system include a clean air source, air heater, mist device, and spiral separator. The top of the mist device comprises three elements. One is a pressure gauge, another is an intake pipe, and the other is the core component nozzle. The spray holes are several uniform round holes with a specific diameter: diameter = $0.4\text{--}1 \text{ mm}$ and number = $3\text{--}5$. The nozzle is connected to an oil suction tube that extends near to the bottom of the oil container. A volume of oil is injected into the oil container, and the temperature-sensing controller controls the heating of the oil bath to a specific temperature. At the same time, in order to minimize the effect of evaporation temperature changes on the fogging concentration, clean compressed air is preheated to $90 \text{ }^\circ\text{C} \pm 2 \text{ }^\circ\text{C}$ using an air heater and then fed into the nozzle atomizer with a nozzle hole at a specific air pressure. Its outlet

is connected to the spiral separator. The separator has a conical right-angle screw which can be moved up and down. Entering the airflow around the screw for circular motion, inertia, and centrifugal force, large particles deposited on the wall along the screw sink to the bottom of the separator. Controlling the degree of separation of oil mist aerosols and regulating the concentration and particle size distribution of oil mist aerosols by rotating the position of the screw up and down, the cross-section area of the airflow channel can be varied within the range of 15–40 mm². The mass average particle size and concentration of the oil mist aerosol that meets the test requirements are finally generated by the coordinated adjustment of all factors.

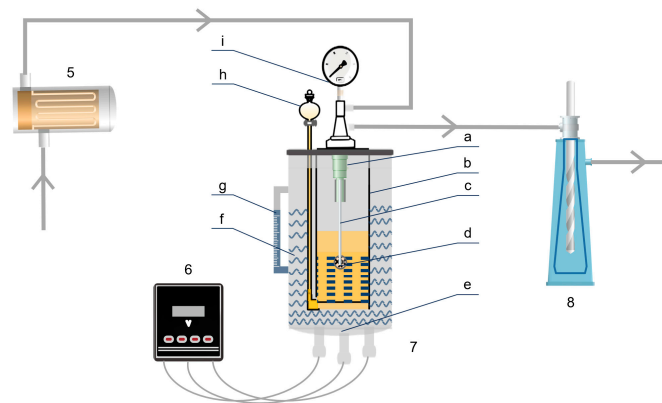


Figure 2. Schematic diagram of oil-mist aerosol generation system. a—Nozzle; b—Oil container; c—Suction hose; d—Steel cover; e—Heating unit; f—Steel oil bath; g—Glass-level meter; h—Oil funnel; i—Barometer.

2.1.3. Filtration Efficiency and Pressure Drop Test System

The two large main pipes connected at both ends of the filter fixture with a high-efficiency filter material are divided into one branch for upstream and downstream aerosol sampling. The mass concentration of aerosol is measured using a luminometer. The sampling ports at both ends of the fixture are connected to a differential pressure meter to detect pressure drop. The test area is set at 20, 50, and 100 cm². We can adjust the gas flow rate from 0 to 50 L/min.

2.1.4. Dilution and Particle-Counting Systems

A dilution system is added to the particle-counting system to prevent the detrimental effects of excessive aerosol concentration on the optical system of the particle-size spectrometer. The sample is taken by the upstream aerosol, and the rotor flowmeter controls the aerosol flow rate. The air compressor provides clean air. The mass flow controller controls clean airflow, and two gases are evenly mixed in the designed mixer. The flow ratio of the original aerosol and clean air during dilution adjusts the dilution ratio. The diluted aerosol was charged by an electrostatic neutralizing device to balance the aerosol charge of Boltzmann and then passed into SMPS for particle size distribution measurement.

2.2. Principle of Filtration Efficiency Test Platform Based on Mass Concentration

The principle of the filtration efficiency test stand based on mass concentration is as follows: under the action of clean compressed air after drying, the airflow passes through the nozzle at a high speed. According to Bernoulli's principle, on the one hand, the high-speed compressed air creates a negative pressure so that the heated oil in the atomizer continuously rises from the suction pipe to the nozzle. On the other hand, the high speed compressed air acts on the oil rising to the nozzle to disperse the oil into oil mist. According to the principle of fluid dynamics, the high-speed fine flow carries the dispersed oil mist, and the sieve at the nozzle removes large droplets; furthermore, small droplets flow out from the atomizer outlet through the gas flow. The aerosols are separated using a spiral

separator, and the large particles are removed under inertia and sedimentation. Oil mist aerosols with different concentrations and particle size distributions can occur by regulating the occurrence conditions. Aerosols are filtered by the pipeline to the filter fixture with high-efficiency filter paper and then filtered into clean gas emissions by HEPA. After the efficient filter, the flowmeter is connected to measure the gas flow through the filter material. The gas flow through the filter material can be controlled by adjusting the bypass airflow, and the control surface flow rate is kept constant. During the experiment, the pressure drop is measured in real time using a differential pressure meter. Aerosol sampling is conducted from the upstream and downstream sampling ports of the filter material fixture. The luminometer measures the mass concentration to calculate the filtration efficiency of the filter material.

3. Materials and Methods

3.1. Experimental Materials and Instruments

32# oil, density of 0.85 g/cm³; kinematic viscosity was 31 and 5.5 mm²/s at 40 °C and 100 °C, respectively (ExxonMobil Inc., Irving, Texas, USA).

Relevant information about experimental instruments is presented in Table 1.

Table 1. Relevant information about experimental instruments.

Instrument Name	Instrument Model	Manufacturer
Polydisperse Aerosol Generator	Non-standard	Beifen Instrument Technology Ltd., Beijing, China
Air Compressor	QWWJ-600	Shanghai Quchen Mechanical and Electrical Technology Co. Ltd., Shanghai, China
Flowmeter	Model 4046	TSI, Shoreview, Minnesota, USA
Electrostatic Neutralizer	1090	
Differential Electric Mobility Shift Screen Instrument	DEMC 2000	PALAS, Karlsruhe, Baden-Württemberg, Germany
Condensation Core Particle Counter	CPC 200	PALAS, Karlsruhe, Baden-Württemberg, Germany

3.2. Experimental Methods

3.2.1. Stability Verification Analysis of Aerosol

A scanning electromobility particle-size spectrometer was used to monitor the particle size distribution spectrum of aerosol particles under the same aerosol occurrence conditions. The scanning time for each group of SMPS is 6 min, scanning was continuously performed for 2 h, and we analyzed the stability of the oil aerosol in the polydisperse aerosol generator analyzed. Relevant parameters of occurrence conditions are presented in Table 2.

Table 2. Relevant parameters about the experiment of stability verification analysis of aerosol.

Type of Parameter	Parameter Name	Unit	Value
Fixed parameter	Oil bath temperature	°C	110
	Injection pressure	MPa	0.10
	Number of nozzles	/	5
	Injection hole size	mm	0.7
	Separation degree	#	3

3.2.2. Influence of Spiral Separation Degree on Particle Size Distribution and Mass Concentration of Aerosol

The degree of separation of the screw separator is changed by adjusting the position of the screw. When the screw separator is not separating, the screw position is set at 0 #. And, the separation degree is 1 # when the screw turns 1 cm down. In that order, the separation degree is 0 #, 1 #, 2 #, 3 #, 4 #, and 5 #. By changing the separation degree of the spiral

separator, aerosols with different particle size distribution and mass concentration are generated. The photometer measured the mass concentration of the aerosol. The particle size distribution of the aerosol is scanned using SMPS for five consecutive scans under each test condition, and the error is analyzed. Relevant parameters of occurrence conditions are presented in Table 3.

Table 3. Relevant parameters about the experiment of influence of spiral separation degree on particle size distribution and mass concentration of aerosol.

Type of Parameter	Parameter Name	Unit	Value
Fixed parameter	Oil bath temperature	°C	100
	Injection pressure	MPa	0.1
	Number of nozzles	/	5
Variable parameter	Injection hole size	mm	0.7
	Separation degree	#	0, 1, 2, 3, 4, 5

3.2.3. Influence of Oil Bath Temperature on Particle Size Distribution and Mass Concentration of Aerosol

By changing the oil bath temperature of the oil mist generator, aerosols with different particle size distributions and mass concentrations are generated. The photometer measured the mass concentration of the aerosol. The particle size distribution of the aerosol is scanned using SMPS for five consecutive scans under each test condition, and the error is analyzed. Relevant parameters of the occurrence conditions are presented in Table 4.

Table 4. Relevant parameters about the experiment of influence of the oil bath temperature on particle size distribution and mass concentration of aerosol.

Type of Parameter	Parameter Name	Unit	Value
Fixed parameter	Injection pressure	MPa	0.1
	Number of nozzles	/	5
	Injection hole size	mm	0.7
Variable parameter	Separation degree	#	1, 3, 5
	Oil bath temperature	°C	80, 90, 100, 110, 120

3.2.4. Influence of Oil Injection Pressure on Particle Size Distribution and Mass Concentration of Aerosol

By changing the oil injection pressure, aerosols with different particle size distributions and mass concentrations are generated. The photometer measured the mass concentration of the aerosol. The particle size distribution of the aerosol is scanned using SMPS for five consecutive scans under each test condition, and the error is analyzed. Relevant parameters of occurrence conditions are presented in Table 5.

Table 5. Relevant parameters about the experiment of influence of oil injection pressure on particle size distribution and mass concentration of aerosol.

Type of Parameter	Parameter Name	Unit	Value
Fixed parameter	Oil bath temperature	°C	100
	Number of nozzles	/	5
	Injection hole size	mm	0.7
Variable parameter	Separation degree	#	1, 3, 5
	Injection pressure	MPa	0.08, 0.10, 0.11, 0.12, 0.13, 0.14

3.2.5. Influence of the Quantity and Size of the Nozzle on the Particle Size Distribution and Mass Concentration of Aerosol

By changing the quantity and size of the nozzle, aerosols with different particle size distributions and mass concentrations are generated. The photometer measured the mass

concentration of the aerosol. The particle size distribution of the aerosol is scanned by SMPS for five consecutive scans under each test condition, and the error is analyzed. Relevant parameters of the occurrence conditions are presented in Table 6.

Table 6. Relevant parameters about the experiment of influence of the quantity and size of the nozzle on the particle size distribution and mass concentration of aerosol.

Type of Parameter	Parameter Name	Unit	Value
Fixed parameter	Oil bath temperature	°C	100
	Separation degree	#	3
	Injection pressure	MPa	0.10
Variable parameter	Number of nozzles	/	3, 5
	Injection hole size	mm	0.4, 0.5, 0.6, 0.7, 0.8

4. Results and Discussion

4.1. Stability Verification Analysis of Oil Mist Aerosol

Whether the oil mist aerosol occurs stably is the basis of the subsequent occurrence condition exploration and filtration efficiency test experiments. Figure 3 shows the particle size distribution of aerosol particles monitored by SMPS. As shown in Figure 3, the oil mist aerosol was normally distributed under the experimental conditions. The particle size distribution range was between 0.02 and 0.8 μm ; most were mainly distributed between 0.06 and 0.3 μm , and the number of aerosol particles peaked at approximately 0.1 μm . The average concentration of the total aerosol from multiple SMPS scans was $1.01 \times 10^8 \text{ P/cm}^3$ with a standard deviation of 7.54×10^5 . The coefficient of variation of the total number of concentration of oil mist aerosol in the generator is 0.748%. The concentration deviation of the peak particle size is less than 1%, indicating that the concentration of the oil mist aerosol in the generator is intact and can be used as a stable source of oil mist aerosol for subsequent occurrence conditions and filter material efficiency tests.

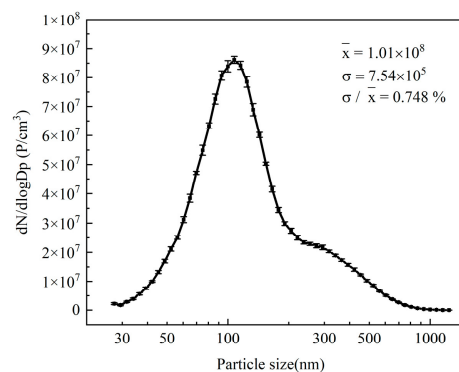


Figure 3. Particle size distribution of generating the aerosols of SMPS continuous scanning for 2 h. \bar{x} —Average value of the total concentration of aerosol particles; σ —standard deviation; σ/\bar{x} —coefficient of variation; occurrence conditions: oil bath temperature 110 °C, injection pressure 0.1 MPa, nozzle number 5, nozzle size 0.7 mm, spiral separation degree 3 #.

4.2. Effect of Spiral Separation Degree on Particle Size Distribution and Mass Concentration of Occurring Aerosol

Figure 4a shows that increased spiral separation decreases the total number of particles and mass concentration. The total number of particles of the oil aerosol decreases from 1.06×10^8 to $7.39 \times 10^7 \text{ P/cm}^3$, and the mass concentration decreases from 1587.9 to 272.1 mg/m^3 . Because the particles in the oil mist move radially outward along the screw under the action of inertial force, they collide on the separator wall and finally deposit at the bottom. The separation effect is more evident for particles with large size and mass. The lower the screw position, the greater the degree of spiral separation. Furthermore, the inertial force acting on the oil mist aerosol and the number of particles removed by the

spiral separation increase. Therefore, the total number of aerosol particles decreases with the increasing degree of spiral separation.

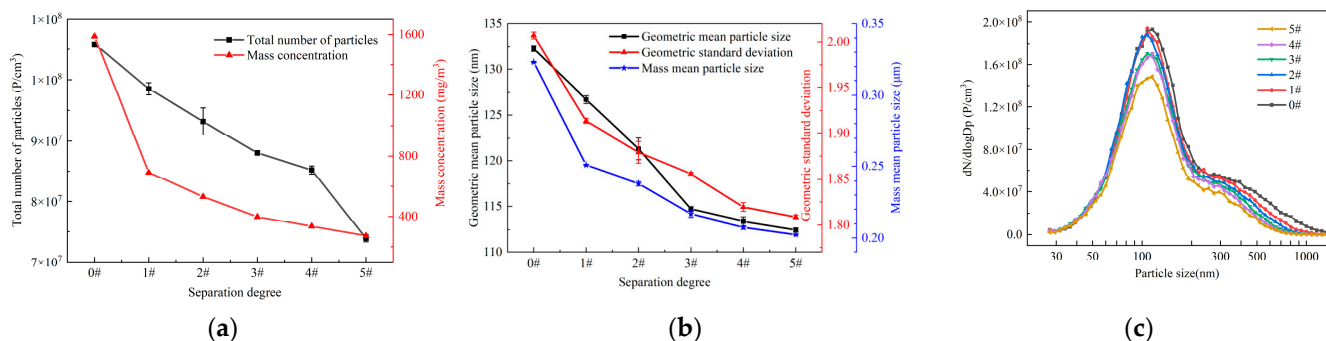


Figure 4. Effects of different separation degrees (a) on the total number and mass concentration of particles (b) on geometric mean particle size, geometric standard deviation and mass mean particle size (c) on particle size distribution. Conditions: oil bath temperature 100 °C, injection pressure 0.1 MPa, nozzle number 5, nozzle size 0.7 mm.

The difference between the number of particles and the mass concentration increases first and then decreases with the increase in the separation degree, which is due to the more significant effect on the large particles under different degrees of spiral separation. Because the large particles have relatively large inertia when the separation degree is increased from 0 # to 1 #, the spiral separator easily removes the particle size and mass of the particles, and the large particles accounted for the larger proportion of the mass, which led to a significant decrease in the mass concentration of aerosol. As the degree of separation increases, the large particles decrease, so the decreasing trend of aerosol mass concentration decreases. The removal of large particles has a small effect on the number of particles, so the number of particles in the early stage of the change is relatively smooth. When the spiral separation range was increased from 4 # to 5 #, the number of particles changed significantly, probably due to the removal of some small particles at this time. Still, the mass concentration did not change significantly due to the small proportion of its mass.

Figure 4b shows that, when the spiral separation degree increases from 0 # to 5 #, as the degree of spiral separation increases, the number of particles removed by the spiral separation increases. The diameter distribution of the remaining particles decreases. The geometric-average particle size, geometric standard deviation and mass-average particle size decrease gradually. The geometric-average particle size of the oil mist aerosol decreases from 132.28 to 112.44 nm. Geometric standard deviation is based on the logarithmic transformation of the data, and it is often used to describe the positive skew distribution of the particle size. The geometric standard deviation decreases from 2 to 1.8, which were polydispersed aerosols. Additionally, the mass-average particle size decreases from 0.32 to 0.20 μm.

Figure 4c shows that the aerosol particle size distribution shrinks as the separation degree increases, and the geometric standard deviation and the polydispersity decrease. Compared with the influence of the number of small particles, the separation degree on large particles is more considerable. This is because particles with large particle sizes and masses have a relatively large inertial effect and are more likely to be removed by the spiral separator when the separation degree increases. Therefore, the geometry and mass mean particle size of aerosols gradually decreases with the separation degree. The mass concentration of aerosols gradually decreases because of the larger particle size of large particulate matter and the large proportion of the mass. As the separation degree increases from 1 # to 5 #, the total number of particles decreases by 24.98%. Furthermore, the mass concentration decreases by 60.68%, indicating that the entire spiral separation process considerably affects the mass concentration, with a slightly smaller impact on the total number of particles. Additionally, most of the removal is of large particles.

4.3. Influence of Oil Bath Temperature on Particle Size Distribution and Mass Concentration of Aerosol

Figure 5a shows that the oil bath temperature considerably affects aerosol development. When the degree of spiral separation is 3 # and the temperature increases from 80 °C to 130 °C, the total particle and mass concentrations of the oil aerosols increase. The degree of separation affects the total number of aerosol particles considerably less than the oil bath temperature. At an oil bath temperature of 100 °C with the degree of spiral separation increasing from 1 # to 5 #, the total number of particles changes by 13.67%. Although the degree of spiral separation is 3 # and the oil bath temperature increases from 80 °C to 130 °C, the total number of particles changes by 61.76%. This may be attributed to the increase in the temperature of oil, resulting in a decrease in viscosity and increased fluidity, which are easily affected by negative pressure. With the increase in the speed of rising through the suction pipe to the spray hole, the amount of oil delivered to the spray hole simultaneously increases, increasing the number of aerosol particles and the mass concentration of oil mist. Furthermore, the figure shows that the lower the degree of separation, the more pronounced the effect of temperature on mass concentration. This may be attributed to the spiral separation–oil bath temperature synergy, decreased separation degree, and reduced aerosol separator path. With increasing temperature, the higher the total number of aerosol particles and mass concentration, the less affected by spiral separation is compared with the whole generation.

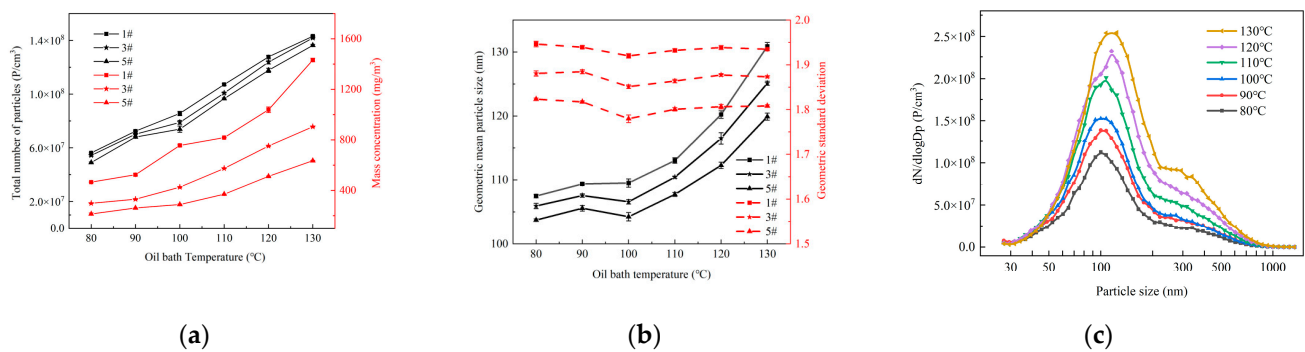


Figure 5. Effects of different oil bath temperature and separation degrees (a) on the total number and mass concentration of particles (b) on geometric mean particle size and geometric standard deviation (c) on particle size distribution of aerosol. Conditions of (a,b): oil injection pressure 0.1 MPa, nozzle number 5, injection hole size 0.7 mm; Conditions of (c): oil injection pressure 0.1 MPa, nozzle number 5, injection hole size 0.7 mm, spiral separation degree 3 #.

Figure 5b,c show that the number of small and large particles increases synchronously with the oil bath temperature, gradually increasing from 80 °C to 100 °C when the degree of separation is 3 #. Additionally, the geometric mean particle size of aerosols fluctuates from 105.91 to 107.55 nm with marginal change. When the temperature exceeds 100 °C, the number of large particles in the aerosol increases considerably higher than that; therefore, the geometric mean particle size increases from 106.58 to 125.12 nm as the oil bath temperature increases from 100 °C to 130 °C. This may be attributed to the mist mechanism of the oil mist generator. For compressed air atomizers, the size distribution of atomization droplets is often used as the Nukiyama–Tanasawa function [22,23] representation:

$$d_0 = \frac{585}{u-v} \left(\frac{\sigma}{\rho} \right)^{0.5} + 597 \left[\frac{\eta}{(\sigma\rho)^{0.5}} \right]^{0.45} \left(1000 \frac{Q_l}{Q_g} \right)^{1.5} \quad (1)$$

where d_0 represents the average diameter of the size distribution of the atomized droplet, u represents the velocity of the compressed air, v represents the velocity of the liquid, σ represents the surface tension of the liquid, ρ represents the density of the liquid, η

represents the dynamic viscosity of the liquid, and Q_l and Q_g represent the volume flow of the liquid and air, respectively.

As shown in Equation (1), the average diameter of atomized droplets in compressed air atomizer is closely related to the surface tension, density and viscosity of the liquid as well as the volume flow ratio of air and the liquid. As the temperature gradually increases, the thermal motion of molecules intensifies and the distance between liquid molecules increases, resulting in a decrease in mutual attraction and a decrease in the liquid viscosity and surface tension. Consequently, the average diameter of atomized droplets gradually increases with increasing temperature.

Furthermore, the increase in the temperature increases the number of aerosol particles, enhances Brownian motion, and increases the probability of aerosol collision, possibly leading to an increase in the number of large particles in the atomized droplets and the overall geometric-average particle size of the aerosols. However, the effect of temperature on the geometric standard deviation is not considerable. Figure 5b shows that the influence of temperature on the geometric mean particle size decreases with increasing separation degree. When the spiral separation degree is 1 #, 3 #, and 5 # and the oil bath temperature increases from 80 °C to 130 °C, the geometric mean particle size increases by 17.89%, 15.35%, and 13.51%, respectively. High temperature causes an increase in the aerosol particle number and geometric mean particle size, and the separator exerts a better removal effect on the particle size and mass. When the separation degree is high, the impact of aerosols at high temperatures is higher than when the separation degree is low. Therefore, the impact of temperature on the geometric mean particle size decreases with the increasing separation degree. Additionally, as the separation degree increases, large particles are more likely to be removed and the geometric standard deviation decreases, resulting in a narrow particle size distribution. Furthermore, the oil bath temperature and spiral separation degree exert a certain influence on the particle size distribution of aerosols and cooperate with the occurrence of oil spray aerosols.

4.4. Influence of Oil Injection Pressure on the Particle Size Distribution and Mass Concentration of Aerosol

Figure 6a,c show that the particle number and mass concentration of the oil spray aerosol increase gradually with increasing oil injection pressure. When the spiral separation degree is 3 #, and the oil injection pressure increases from 0.08 to 0.14 MPa, the total number of particles of the aerosol increases from 8.99×10^7 to 1.63×10^8 P/cm³, and the mass concentration increases from 387.8 to 542.2 mg/m³. In atomization, the droplet number flux represents the number of droplets passing per unit time per unit area, and the expression for this flux is as follows [24,25]:

$$N = \frac{6Q}{\pi d_0^3 S} \quad (2)$$

where N denotes the flux of the droplet, Q denotes the volume flow of the nozzle, and S denotes the spray cover area.

When the nozzle parameters are unchanged, the spray coverage area remains unchanged, and the increase in injection pressure leads to an increase in the volume flow through the nozzle. Therefore, the flux of oil mist droplets increases, and the number of particles in the oil spray aerosol increases. In addition, when the injection pressure increases, the liquid is more likely to be broken into small droplets by the gas pressure, which is conducive to the rise in the number of particles. The increase in the particle number will also cause an increase in the mass concentration of the oil mist.

The degree of spiral separation exerts less effect on the particle number concentration than the effect of the jet pressure. This may be because, when the injection pressure increases, most of the increased particles have a small particle size, and the spiral separation does not have a noticeable effect on the small particle size, making the spiral separation degree exert a marginal impact on the number concentration of particles. The effect of injection pressure on mass concentration decreases with increasing separation. This is because although the

increase in injection pressure increases the concentration of particles, it also increases the speed of the separator and the spiral separation effect, increasing the number of particles removed during separation, particularly the number of particles with a large mass. In the case of a low separation degree, the pressure dominates the particle number concentration. In the case of a high separation degree, the separation effect dominates, the removal effect of the large particles is more obvious, and the mass concentration is reduced. Therefore, the overall mass concentration of the oil mist aerosol does not change considerably.

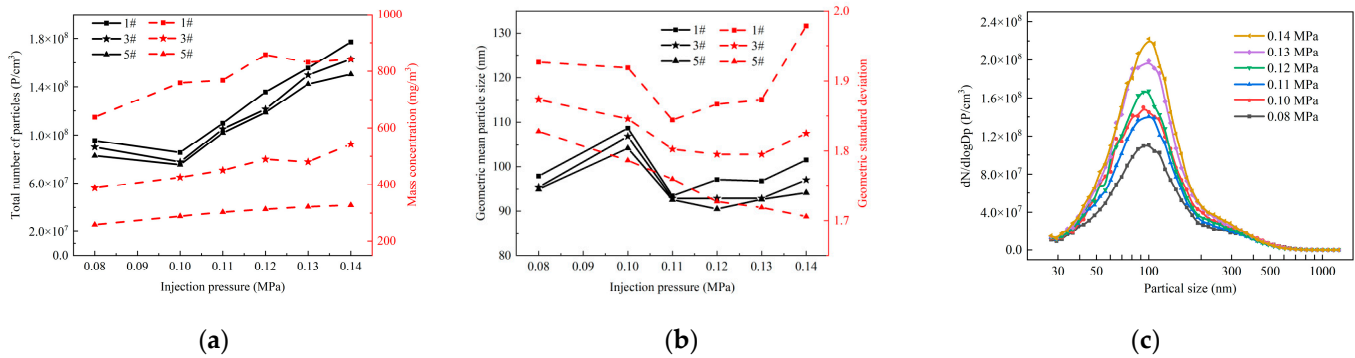


Figure 6. Effect of different injection pressure and separation degrees (a) on the total number and mass concentration of particles (b) on geometric mean particle size and geometric standard deviation (c) on particle size distribution of aerosol. Conditions: oil bath temperature 100 °C, nozzle number 5, nozzle size 0.7 mm.

Figure 6b shows that, as the oil injection pressure increases, the geometric average particle size of the oil mist aerosol initially increases and then decreases. The increase in the oil injection pressure leads to an increase in gas flow. As shown in Equation (1), the increase in gas flow leads to a decrease in the ratio of liquid and gas flow, thereby reducing the average particle size of droplets. Moreover, the geometric standard deviation gradually decreases with increasing injection pressure when the separation degree is high. When the separation degree is low, the geometric standard deviation initially decreases and increases with increasing injection pressure. This is because when the oil injection pressure increases, the aerosol velocity through the separator increases, and the removal of large particles is more considerable. The higher the separation degree, the greater the removal effect, resulting in the gradually narrow particle size distribution. When the separation degree is low with a low oil injection pressure, the removal of particulate matter is small, making the geometric standard deviation large. When the pressure gradually increases, the removal effect of the separator increases, resulting in a decrease in the geometric standard deviation.

Moreover, the pressure continues to increase, and the increase in the number of aerosol particles is stronger than the removal effect of the separator. Therefore, the geometric standard deviation increases. The injection pressure of the aerosol affects its mass concentration and particle size distribution; thus, the influence of the injection pressure on the particle size and mass distribution of the aerosol is complicated. Accordingly, investigating the characteristics of the aerosol injection pressure of the generator is essential.

4.5. Influence of the Quantity and Size of the Nozzle on the Particle Size Distribution and Mass Concentration of the Occurring Aerosol

Figure 7a shows that for the three-hole nozzle and five-hole nozzle, the aerosol flow rate increases linearly with the increase in the nozzle size. Figure 7b shows that, when the size of the three-hole nozzle rises from 0.4 to 0.8 mm, the total number of aerosol particles increases from 5.88×10^7 to 8.42×10^7 P/cm^3 . However, the mass concentration of the aerosol decreases from 1552.0 to 435.3 mg/m^3 .

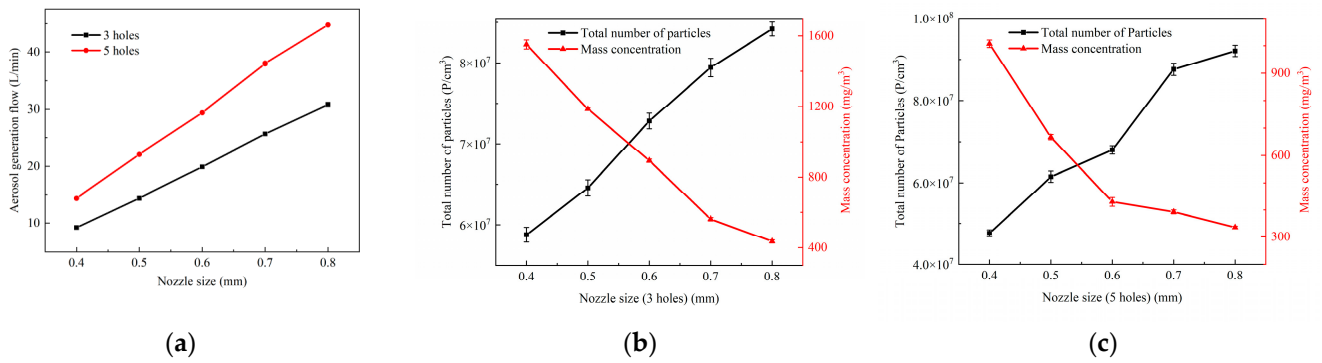


Figure 7. Effects of different nozzle sizes (a) on aerosol generation flow rate (b) on the total number of particles and mass concentration (3 holes) (c) on the total number of particles and mass concentration (5 holes). Occurrence conditions: oil bath temperature 100 °C, spiral separation degree 3 #, oil injection pressure 0.10 MPa.

Figures 8a and 9a show that the number of small particles in the oil aerosol increases considerably more than the number of large particles with increasing nozzle size. The overall particle size distribution of the aerosol slightly shifts to the left, and the geometric-average particle size decreases from 127.42 to 103.06 nm. The reason for this phenomenon may be that when the nozzle size increases, the gas flow through the nozzle increases, and the oil drop at the nozzle has a large momentum, which is more conducive to the impact of the breaking agent into smaller droplets, resulting in a decrease in the overall particle size of the aerosol along with an increase in the nozzle size [26,27]. Furthermore, when the aerosol flow rate increases, the number of large particles removed by impact and other actions through the spiral separator is greater than that of small particles. Therefore, the overall particle size of the oil mist aerosol decreases with increasing nozzle size. The number and mass concentration of aerosol particles occurring for the different sizes of five-hole nozzle and 3-hole nozzle have the same trend.

As shown in Figure 8, the geometric standard deviation of aerosols generated from three-hole and five-hole nozzles also decreases with increasing nozzle size because of the improvement in removing the aerosol polydispersity. For the 5-hole nozzles of different sizes, the change in aerosol geometric average particle size is less obvious than that of the three-hole nozzle. Because the flow rate through the five-hole nozzle is larger than that through the three-hole nozzle and the spiral separation effect is more obvious, the overall geometric average particle size is small.

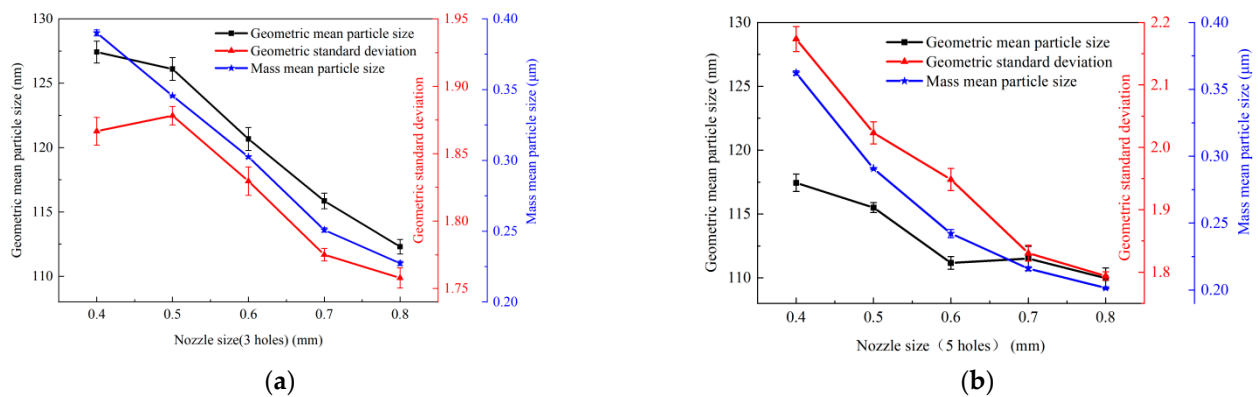


Figure 8. Effect of the nozzle size on geometric mean diameter, geometric standard deviation, and mass mean diameter for the (a) 3-hole nozzle and (b) 5-hole nozzle. Occurrence conditions: oil bath temperature 100 °C; spiral separation degree 3 #; and oil injection pressure 0.10 MPa.

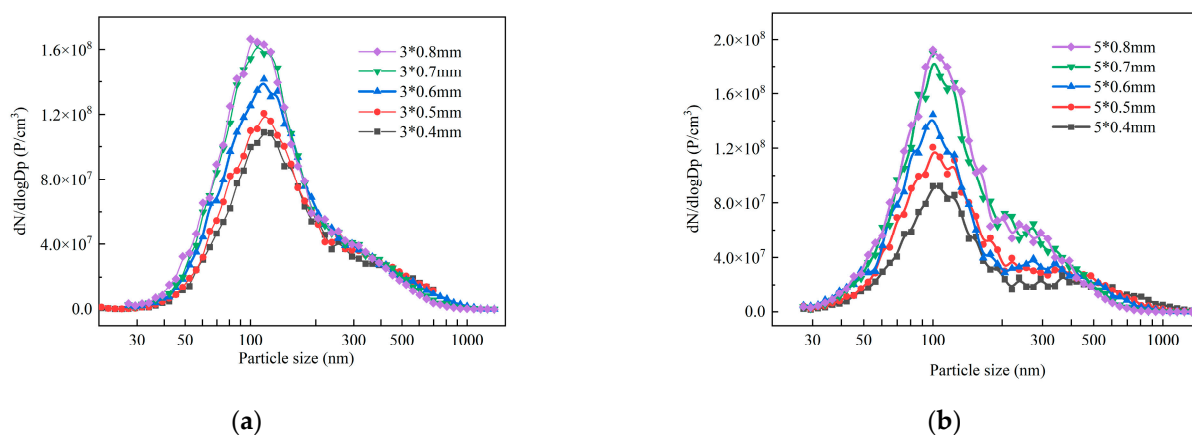


Figure 9. Effect of nozzle size on particle size distribution of aerosol for the (a) 3-hole nozzle and (b) 5-hole nozzle. Occurrence conditions: oil bath temperature 100 °C; spiral separation degree 3 #; oil injection pressure 0.10 MPa.

An aerosol with a higher mass concentration can occur due to the geometric standard deviations of the three-hole nozzle being less than that of the five-hole nozzle. The number and size of the nozzle are smaller, the gas flow has less influence on aerosol properties, and the conditions can be adjusted more stably to achieve the ideal occurrence state. Therefore, in the subsequent experiments, a three-hole nozzle can be selected for aerosol occurrence to meet the requirements of the filter material detection standards. The average particle size of the aerosol mass used as specified in GB 6165-2021 ranges from 0.28 to 0.34 μm . As shown in Figure 8a, the average particle size of the aerosol can be controlled within the range when the oil bath temperature is 100 °C, the separation degree is 3 #, the oil injection pressure is 0.10 MPa, and the size of the three-hole nozzle is 0.5 or 0.6 mm. Additionally, at 0.6 mm, the total particle number and mass concentration of the aerosol are higher, which can make the upstream aerosol reach a high concentration, thereby expanding the filter grade test range of the test stand. If other size nozzles are selected, the particle size can be controlled within the standard range by adjusting different parameters.

5. Conclusions

This study designed and built a filtration efficiency test system for high-efficiency filter materials that can generate high-concentration aerosols based on mass concentration. We analyzed the stability of the oil aerosol, and determined the conditions for aerosol occurrence. The main results of this study are summarized as follows.

A filtration efficiency test system for high-efficiency filter materials based on mass concentration is designed and built. The test stand can stably produce an aerosol with a mass concentration of up to 1587.9 mg/m^3 and a number concentration of up to 1.63×10^8 P/cm^3 .

The occurrence state of the aerosol is affected by different occurrence conditions. The degree of spiral separation increases from 0 # to 5 #; the mass concentration decreases from 1587.9 to 272.1 mg/m^3 ; and the geometric mean particle size decreases. The oil bath temperature increases from 80 °C to 130 °C, the total concentration of aerosol particles increases to 1.42×10^8 P/cm^3 , and the mass concentration increases to 904.0 mg/m^3 . The injection pressure cooperates with the spiral separation degree. The nozzle size exerts the opposite effect on the total number of particles and the mass concentration. When the three-hole nozzle size increases from 0.4 to 0.8 mm, the total number of particles of oil aerosol increases from 5.88×10^7 to 8.42×10^7 P/cm^3 . However, the mass concentration decreases to 435.3 mg/m^3 .

The aerosol generation conditions of the generator are determined: the number of nozzles is three; the nozzle diameter is 0.5 or 0.6 mm; the oil bath temperature is 100 °C; and the oil injection pressure is 0.1 MPa. The spiral separation position is adjusted according to the average mass size; furthermore, the particle size ranges from 0.28 to 0.34 μm , and

the mass concentration ranges from 900 to 1000 mg/m³. The aerosol particle number concentration is approximately 7×10^7 P/cm³. All these results meet the requirements of GB 6165-2021 test standards.

Author Contributions: Methodology, F.W. and M.H.; validation, F.W.; investigation, M.H.; data curation, F.W.; writing—original draft preparation, F.W.; writing—review and editing, H.W. and M.T.; supervision, Y.L.; project administration, L.W. and D.W. All authors have read and agreed to the published version of the manuscript.

Funding: This research received no external funding.

Data Availability Statement: Data will be made available upon request.

Conflicts of Interest: The authors declare no conflicts of interest.

References

1. Tong, X.; Wang, B.; Dai, W.T. Indoor air pollutant exposure and determinant factors controlling household air quality for elderly people in Hong Kong. *Air Qual. Atmos. Health* **2018**, *11*, 695–704. [[CrossRef](#)]
2. Landrigan, P.J. Air pollution and health. *Lancet Public Health* **2017**, *2*, 4–5. [[CrossRef](#)] [[PubMed](#)]
3. Xue, Y.; Wang, L.; Zhang, Y.; Zhao, Y.; Liu, Y. Air pollution: A culprit of Lung Cancer. *J. Hazard. Mater.* **2022**, *434*, 128937. [[CrossRef](#)]
4. Yao, L.; Zhan, B.; Xian, A. Contribution of transregional transport to particle pollution and health effects in Shanghai during 2013–2017. *Sci. Total Environ.* **2019**, *677*, 564–570. [[CrossRef](#)] [[PubMed](#)]
5. Dockery, D.W. Health effects of particulate air pollution. *Ann. Epidemiol.* **2009**, *19*, 257–263. [[CrossRef](#)] [[PubMed](#)]
6. Mahowald, N. Aerosol indirect effect on biogeochemical cycles and climate. *Science* **2011**, *334*, 794–796. [[CrossRef](#)]
7. Lee, K.W.; Liu, B.Y.H. Theoretical study of aerosol filtration by fibrous filters. *Aerosol Sci. Technol.* **1982**, *1*, 147–161. [[CrossRef](#)]
8. Hutten, I.M. (Ed.) Chapter 2—Filtration mechanisms and theory. In *Handbook of Nonwoven Filter Media*, 2nd ed.; Butterworth-Heinemann: Oxford, UK, 2016; pp. 53–107.
9. Jung, S.; Kim, J. Advanced design of fiber-based particulate filters: Materials, morphology, and construction of fibrous assembly. *Polymers* **2020**, *12*, 1714. [[CrossRef](#)] [[PubMed](#)]
10. Mandal, S.; Pathak, M.P.; Sharma, B.N.; Patowary, P.; Barman, P.K.; Kishor, S.; Goyary, D.; Verma, N.; Chattopadhyay, P. Determination of LCt50 of aerosolized paraquat and its pulmonary toxic implications in non-anesthetized rats. *Drug Chem. Toxicol.* **2019**, *42*, 552–558. [[CrossRef](#)]
11. Tang, M.; Chen, S.C.; Pui, D.Y.H. An improved atomizer with high output of nanoparticles. *J. Aerosol Sci.* **2018**, *124*, 10–16. [[CrossRef](#)]
12. Eninger, R.M.; Honda, T.; Reponen, T. What does respirator certification tell us about filtration of ultrafine particles. *J. Occup. Environ. Hyg.* **2008**, *5*, 286–295. [[CrossRef](#)] [[PubMed](#)]
13. Stevens, G.A.; Moyer, E.S. “Worst case” aerosol testing parameters: I. Sodium chloride and dioctyl phthalate aerosol filter efficiency as a function of particle size and flow rate. *Am. Ind. Hyg. Assoc. J.* **1989**, *50*, 257–264. [[CrossRef](#)] [[PubMed](#)]
14. Li, L.; Zuo, Z.; Japuntich, D.A. Evaluation of filter media for particle number, surface area and mass penetrations. *Ann. Occup. Hyg.* **2012**, *56*, 581–594. [[PubMed](#)]
15. Zhang, Z.; Jiang, F. In-place HEPA filter testing by the sodium flame method. *Powder Technol.* **2016**, *301*, 615–621. [[CrossRef](#)]
16. Dhaniyala, S.; Liu, B. Investigations of particle penetration in fibrous filters: Part I. Experimental. *J. IEST* **1999**, *42*, 32–40. [[CrossRef](#)]
17. Japuntich, D.A.; Franklin, L.M.; Pui, D.Y.; Kuehn, T.H.; Kim, S.C.; Viner, A.S. A Comparison of two nano-sized particle air filtration tests in the diameter range of 10 to 400 nanometers. *J. Nanoparticle Res.* **2007**, *9*, 93–107. [[CrossRef](#)]
18. Liu, B.Y.H.; Rubow, K.L.; Pui, D.Y.H. Performance of HEPA and ULPA filters. In *Proceedings, Annual Technical Meeting—Institute of Environmental Sciences*; Institution of Environmental Sciences: London, UK, 1985; pp. 25–28.
19. Zhang, Z.; Wei, J.; Jiang, F.; Yu, T. Testing methods for counting efficiency of EPA/HEPA/ULPA filter media. *J. Tsinghua Univ. (Sci. Technol.)* **2010**, *50*, 422–425.
20. Wang, D. Study on Structure and Properties of Coalescent Materials for Oil/Gas Separation. Master’s Dissertation, South China University of Technology, Guangzhou, China, 2019.
21. GB 6165; High Efficiency Air Filter Performance Test Method Efficiency and Resistance. Standards Press of China: Beijing, China, 2021.
22. Nkiyama, S. Experiments on the atomization of liquids in an air stream, report 3, on the droplet-size distribution in a atomized jet. *Trans. Soc. Mech. Eng. Jpn.* **1939**, *5*, 62–67.
23. Mikuška, P. Generator of fine polydisperse aerosol. *Collect. Czechoslov. Chem. Commun.* **2004**, *69*, 1453–1463. [[CrossRef](#)]
24. Wang, S.; Zhen, M.; Wu, Z. Numerical Simulation of Effect of Pressure on Atomization Characteristics of Nozzle. *Mach. Des. Manuf.* **2020**, *3*, 51–54.

25. Wu, Z.; Zhen, M.; Liu, M. Analysis of influencing factors on atomization Characteristics of hollow cone pressure swirl Nozzle. *Chin. J. Power Eng.* **2018**, *38*, 988–995.
26. Zaremba, M.; Weiß, L.; Malý, M.; Wensing, M.; Jedelský, J.; Jícha, M. Low-pressure twin-fluid atomization: Effect of mixing process on spray formation. *Int. J. Multiph. Flow* **2017**, *89*, 277–289. [[CrossRef](#)]
27. Jing, D.; Zhang, F.; Li, Y.; Xu, H.; Shuai, S. Experimental investigation on the macroscopic and microscopic spray characteristics of diesel fuel. *Fuel* **2017**, *199*, 478–487. [[CrossRef](#)]

Disclaimer/Publisher’s Note: The statements, opinions and data contained in all publications are solely those of the individual author(s) and contributor(s) and not of MDPI and/or the editor(s). MDPI and/or the editor(s) disclaim responsibility for any injury to people or property resulting from any ideas, methods, instructions or products referred to in the content.